

In vivo imaging of heart failure with preserved ejection fraction by simultaneous monitoring of cardiac nitric oxide and glutathione using a three-channel fluorescent probe

Xiao-Xiao Chen ^{a,1}, Yufei Wu ^{b,1}, Xiaoxiao Ge ^c, Liandi Lei ^{b,d}, Li-Ya Niu ^{a, **}, Qing-Zheng Yang ^{a, *}, Lemin Zheng ^{b, ***}

^a Key Laboratory of Radiopharmaceuticals Ministry of Education, College of Chemistry, Beijing Normal University, Beijing, 100875, China

^b The Institute of Cardiovascular Sciences and Institute of Systems Biomedicine, School of Basic Medical Sciences, Key Laboratory of Molecular Cardiovascular Science of Ministry of Education, NHC Key Laboratory of Cardiovascular Molecular Biology and Regulatory Peptides, Beijing Key Laboratory of Cardiovascular Receptors Research, Health Science Center, Peking University, Beijing, 100191, China

^c Beijing Institute of Brain Disorders, Capital Medical University, Beijing, 100069, China

^d Center of Medical and Health Analysis, Peking University, Beijing, 100191, China



ARTICLE INFO

Keywords:

Fluorescent probe
Oxidative stress
Heart failure

ABSTRACT

The pathophysiology of heart failure with preserved ejection fraction (HFpEF) remains unclear, making the diagnosis and treatment challenging. Cardiac oxidative and nitrative stress are strongly implicated in the pathogenesis of HFpEF. Herein, we present a unique three-channel fluorescent probe for evaluating cardiac oxidative and nitrative stress in HFpEF by simultaneous detection of NO and GSH. The probe exhibits a native green fluorescence (probe channel), while the presence of GSH and NO can sensitively turn the native green fluorescence into red fluorescence (GSH channel) and near-infrared fluorescence (NO channel), respectively. The probe clearly reveals that both GSH and NO levels are upregulated in cardiomyocytes and heart tissue with HFpEF. Moreover, it uncovers that the enhancement in NO and GSH levels are closely associated with increased level of iNOS (inducible nitric oxide synthase) and activation of the Keap1 (Kelch-like ECH-associated protein 1)/Nrf2 (nuclear factor erythroid 2-related factor 2)/ARE (antioxidant response element) signaling pathway in cardiomyocytes, respectively. This work proposes a promising approach for distinguishing normal heart and HFpEF heart by *in vivo* noninvasive imaging of both GSH and NO, and greatly contributing to the improvement of the diagnosis and treatment of HFpEF.

1. Introduction

Heart failure with preserved ejection fraction (HFpEF) has gradually become the main form of heart failure, accompanied the substantial morbidity and mortality (Borlaug 2014; Shah Amil et al., 2017). Due to its complexity and heterogeneity in the features of HFpEF, the diagnosis and treatment are facing huge challenges (Borlaug 2020; Dunlay et al., 2017). Several diagnostic algorithms have been proposed, while their specificities and sensitivities are widely different for diagnosing HFpEF (McDonagh et al., 2021). Moreover, there is no convincing effective treatment toward reducing mortality and morbidity in patients with

HFpEF. Thus, the establishment of an effective method for uncovering the underlying mechanism of HFpEF is essential to improve diagnosis accuracy for HFpEF and to advance the clinical therapy.

Nitrative and oxidative stress are closely linked to inflammatory activation that has been historically recognized as a primary contributor to the pathogenesis of HFpEF (Mishra and Kass, 2021). Schiattarella et al. ever proved that the increasing activity of inducible nitric oxide synthase (iNOS) in cardiomyocytes can promote the progression of HFpEF via inducing the protein nitration in cardiomyocytes and the followed cardiac diastolic dysfunction (Schiattarella et al., 2019). However, the previous study on the activity of iNOS relies on invasive

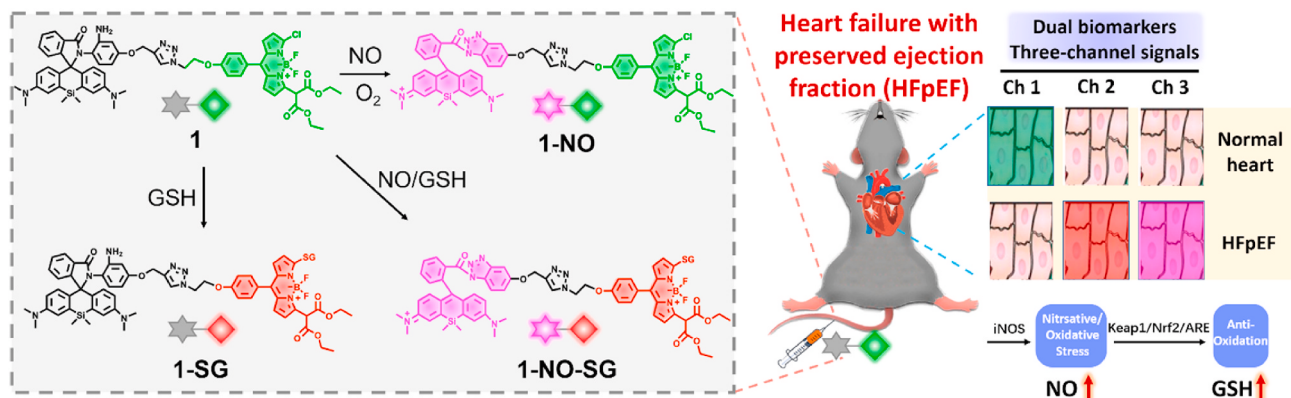
* Corresponding author.

** Corresponding author.

*** Corresponding author.

E-mail addresses: niuly@bnu.edu.cn (L.-Y. Niu), qzyang@bnu.edu.cn (Q.-Z. Yang), zhengl@bjmu.edu.cn (L. Zheng).

¹ These authors contributed equally to this work.



Scheme 1. Schematic illustration of probe 1 to detection NO and GSH through three fluorescence signals for imaging HFpEF heart over normal heart.

analysis techniques *in vitro*. Nitric oxide (NO) is an essential mediator in the process of iNOS-induced nitrosative stress imbalance (Yu et al., 2018). The direct visualization of NO levels *in situ* will be more beneficial to provide detailed information on the pathogenesis of HFpEF. On the other hand, organisms possess a variety of antioxidant systems to counteract the oxidative stress and maintain redox balance (Birben et al., 2012). Glutathione (GSH) is the most abundant cellular thiolic antioxidant that can effectively protect cell against the oxidative stress (Campos et al., 2013). The monitor of GSH changes is important for comprehensive studying cellular redox state (Jiang et al., 2017). Considering the serious complications of HFpEF in clinics, synergistical targeting both NO and GSH would provide a more precise method for

specifically evaluating the cardiac oxidative and nitrosative stress, which will be helpful for the diagnosis and treatment of HFpEF.

Molecular imaging, as a noninvasive method, can achieve real-time detection of the onset and progression of diseases in living organisms. Conventional diagnostic technologies, including magnetic resonance imaging (MRI), cardiac computed tomography (cardiac CT), single-photon emission computed tomography (SPECT), positron emission tomography (PET) and echocardiography, mainly provide the detailed anatomic and functional changes of heart. Compared with them, the fluorescent probes are featured with many benefits, such as high sensitivity, superior selectivity, non-destructive imaging. Utilizing fluorescent probe to detect living metabolites *in vivo* has been served as an

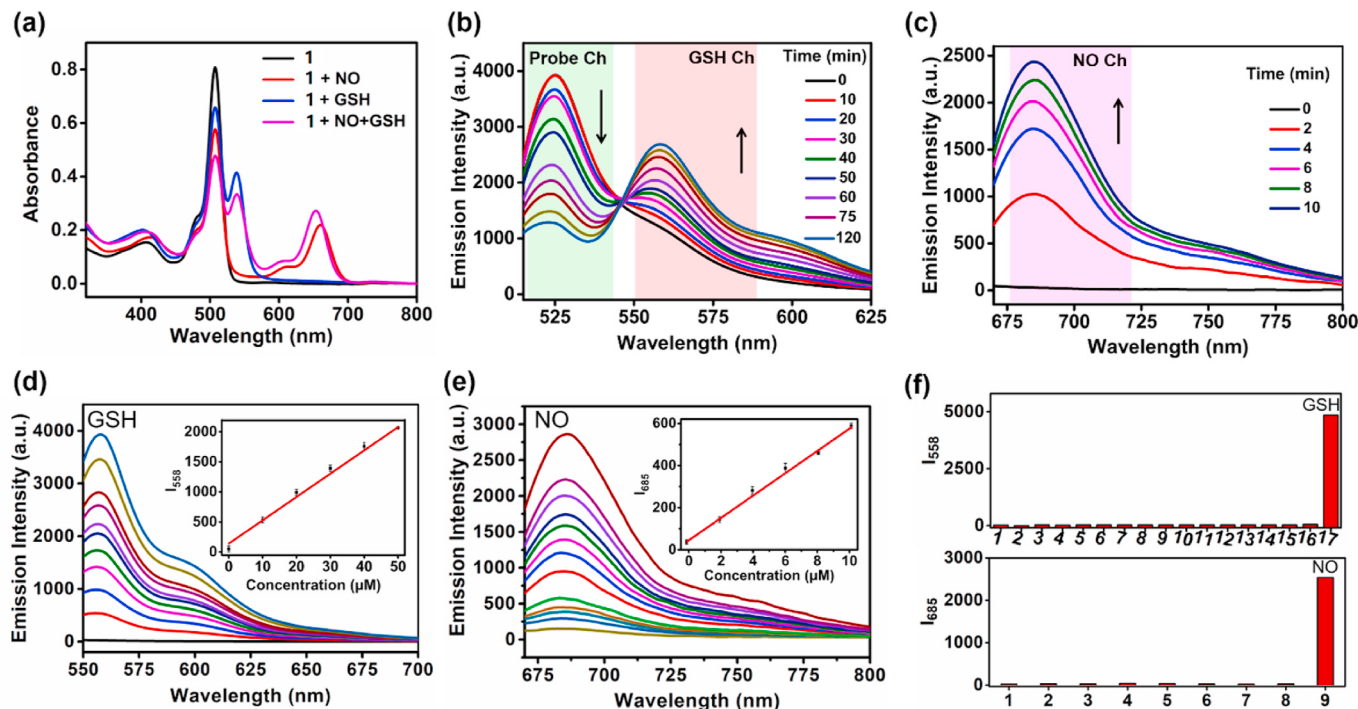


Fig. 1. Photophysical properties of probe 1 exposed in NO and GSH standard solution. (a) Absorbance spectra of probe 1 in the presence of DEA-NO₂Oate (1 mM) and GSH (1 mM). (b, c) Real-time fluorescence spectra of probe 1 in both GSH (200 μ M) and DEA-NO₂Oate (200 μ M) solution under three different excitation wavelengths (λ_{ex}): (b) λ_{ex} = 508 nm, (c) λ_{ex} = 660 nm. (d) Fluorescence spectra of probe 1 (10 μ M) treated with increasing concentration of GSH (0–200 μ M) for 1 h λ_{ex} = 540 nm, λ_{em} = 558 nm. (Inset: corresponding linear relationship between the fluorescent intensity and GSH concentration, R^2 = 0.996). (e) Fluorescence spectra of probe 1 (10 μ M) treated with different concentration of DEA-NO₂Oate (0–200 μ M) for 30 min λ_{ex} = 660 nm, λ_{em} = 685 nm. (Inset: corresponding linear relationship between the fluorescent intensity and DEA-NO₂Oate concentration, R^2 = 0.995). (f) Fluorescence intensity of probe 1 (10 μ M) coincubated with various amino acids and species containing sulfur for 2 h (λ_{ex} = 540 nm, λ_{em} = 558 nm). Legend: 1, blank; 2, SO_4^{2-} ; 3, SO_3^{2-} ; 4, $\text{S}_2\text{O}_8^{2-}$; 5, $\text{S}_2\text{O}_8^{2-}$; 6, HSO_4^- ; 7, HSO_3^- ; 8, HS^- ; 9, His; 10, Iso; 11, Leu; 12, Lys; 13, Met; 14, Ser; 15, Cys; 16, Hcy; 17, GSH. (g) Fluorescence intensity of probe 1 coincubated with different reactive oxygen species and reactive nitrogen species for 10 min (λ_{ex} = 660 nm, λ_{em} = 685 nm). Legend: 1, blank; 2, NO_3^- ; 3, NO_2^- ; 4, O_2^- ; 5, OH^- ; 6, H_2O_2 ; 7, $\text{O}_2\cdot$; 8, ONOO^- ; 9, DEA-NO₂Oate.

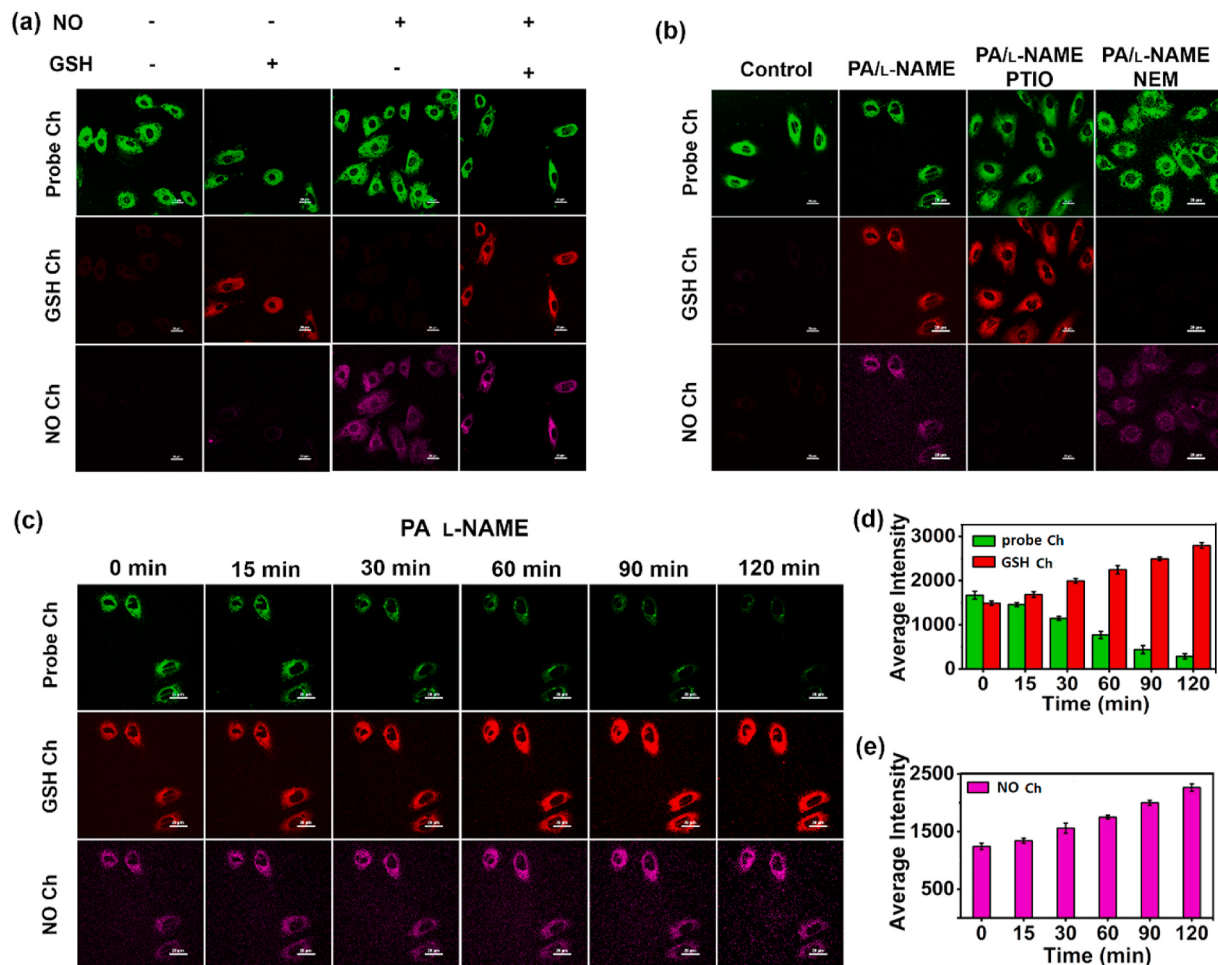


Fig. 2. *In Vitro* confocal fluorescence images of cellular NO and GSH using probe **1** in H9C2 Cells. (a) First column: cells incubated with NEM (0.5 mM, 30 min) and then **1** (10 μ M, 20 min); second column: cells incubated with **1** (10 μ M, 20 min); third column: NEM-loaded cells stained with DEA-NOONate (200 μ M, 20 min) and then **1** (10 μ M, 20 min); fourth column: cells pretreated with DEA-NOONate (200 μ M, 20 min) and then **1** (10 μ M, 20 min). (b) first column: normal H9C2 cells incubated with **1** (10 μ M, 20 min); second column: cells in PA/L-NAME group pretreated with **1** (10 μ M, 20 min); third column: cells in PA/L-NAME group incubated with PTIO (0.5 mM, 30 min), and further treated with **1** (10 μ M, 20 min); fourth column: cells in PA/L-NAME group treated with NEM (0.5 mM, 30 min), and further loaded with **1** (10 μ M, 20 min). (c) Real-time confocal fluorescence images of H9C2 cells in PA/L-NAME group incubated with **1** (10 μ M, 20 min). (d, e) Average fluorescence intensity of probe, GSH and NO channels. Fluorescence images from probe channel ($\lambda_{\text{ex}} = 487$ nm, $\lambda_{\text{em}} = 500\text{--}530$ nm), GSH channel ($\lambda_{\text{ex}} = 487$ nm, $\lambda_{\text{em}} = 557\text{--}590$ nm) and NO channel ($\lambda_{\text{ex}} = 638$ nm, $\lambda_{\text{em}} = 670\text{--}720$ nm). Scale bar: 20 μ m.

attractive tool for visualizing complex biological dynamic processes (Chen et al., 2016; Erbas-Cakmak et al., 2018; Fernández and Vendrell, 2016; Niu et al., 2015; Park et al., 2020; Su et al., 2017; Wang et al., 2021; Wu et al., 2021; Yue et al., 2019). Although fluorescent probes for the detection of NO (Finney, 2006; Huo et al., 2019; Lim and Lippard, 2007; Lim et al., 2006; Lucero et al., 2021; McQuade et al., 2010; Qi et al., 2021; Sasaki et al., 2005; Teng et al., 2019; Ye et al., 2020; Zhou et al., 2020) or GSH (Bhuniya et al., 2014; Jiang et al., 2017; Kang et al., 2019; Kong et al., 2016; Liu et al., 2020; Morozumi et al., 2020; Niu et al., 2012; Tian et al. 2020a, 2020b; Umezawa et al., 2016; Yin et al., 2015, 2017) have been developed individually, it still lacks of a single probe which enable to target NO and GSH simultaneously. There are only two reported fluorescent probes (Chen et al., 2019) (Chen et al., 2021) developed by our group have been developed by attaching NO and GSH reaction sites into a single fluorophore. Unfortunately, they cannot independently response to NO and GSH. The spectral overlap when response to NO and GSH would make it difficult to accurately monitor NO and GSH. To the best of our knowledge, no fluorescent probes which is capable of independently imaging NO and GSH has been reported. Such systems would allow synergistically target both two species in the process of HFpEF and potentially provides a more specific imaging signal for evaluating the cardiac redox status.

In this work, a fluorescent probe **1** is developed for *in vivo* real-time imaging of HFpEF by monitoring NO and GSH levels in mice hearts with three distinct fluorescence channels (Scheme 1). Probe **1** consists of two fluorescent moieties with widely separated emission signals and capable of independent detection of NO and GSH, respectively. **1** possesses native green fluorescence (Ch 1). In the presence of GSH and NO, it exhibits red fluorescence (Ch 2) and near-infrared (NIR) fluorescence (Ch 3), respectively. The *in vitro* and *in vivo* imaging revealed that the concentrations of NO and GSH increased simultaneously in cardiomyocytes and hearts of mice model with HFpEF. Furthermore, our results demonstrated that excess NO was induced by the upregulation of iNOS and the increase of GSH levels was associated with activation of the Keap1/Nrf2/ARE antioxidant pathway in cardiomyocytes. Thus, this work provides a new molecular tool for imaging cardiac stress of HFpEF and proposes a new perspective for understanding the pathogenesis of HFpEF, thus contributing to HFpEF diagnosis and treatment.

2. Results and discussion

2.1. Design and principle of three-channel fluorescent probe for simultaneous detection of GSH and NO

To achieve simultaneous and independent detection of NO and GSH, the probe is composed of two molecule-responsive unites, Si-rhodamine with *o*-phenylenediamine (OPD) and monochlorinated BODIPY (Scheme 1). Si-rhodamine and BODIPY possess excellent photophysical properties, including brilliant quantum yield, high extinction coefficients and great photostability (Boens et al., 2012; Liu et al., 2016). In addition, the emission wavelengths of Si-rhodamine (~685 nm) and BODIPY (~525 nm) fluorophores are well separated without spectral overlap, thereby avoiding signal crosstalk. Si-rhodamine with OPD did not exhibit any fluorescence due to the “OPD-locked” spirolactam, while another unit of monochlorinated BODIPY had obviously native green fluorescence. Thus, the probe 1 itself exhibited green fluorescence (probe Ch). When in the presence of GSH, the chlorine of monochlorinated BODIPY can be replaced through a “ S_N Ar-rearrangement” mechanism to form a sulfur-substituted BODIPY (1-SG) with a red-shifted fluorescence emission (GSH channel) (Kang et al., 2019; Niu et al., 2012). While NO existed, the “OPD-locked” spirocyclic form was broken by ring-opening reaction to form 1-NO, thus generating an enhanced NIR emission (NO channel) (Boens et al., 2012; Liu et al., 2016). Thus, the designed three-channel probe can monitor both NO and GSH simultaneously. Probe 1 was synthesized and characterized by 1 H and 13 C NMR spectroscopy and high-resolution mass spectrometry (HRMS) (See Supporting Information).

2.2. Photophysical response of probe towards NO and GSH

With probe 1 in hand, we investigated the spectral properties of 1 towards NO and GSH. As shown in Fig. 1a, free 1 manifests an absorption maximum at 508 nm and a fluorescence peak at 525 nm from the BODIPY fluorophore. Upon addition of DEA-NONOate (a commercial NO donor), an absorption peak at around 660 nm emerged. Meanwhile, a significant fluorescence enhancement was observed at 685 nm, suggesting a ring-opening of the Si-rhodamine moiety in the presence of NO (Fig. S1a). HRMS experiments were utilized to demonstrate the formation of 1-NO (Fig. S15). Upon addition of GSH, the absorption intensity at 508 nm decreased gradually, while the absorption intensity at 540 nm increased. A new fluorescence peak centered at 558 nm appeared (Fig. S1b). According to our previous works, this peak is assigned to 1-SG, which was confirmed by HRMS experiments (Fig. S16). When NO and GSH coexisted in solution, both the absorption peaks at 525 nm and 660 nm can be observed, suggesting 1-NO-SG was generated. Moreover, HRMS experiments further identified the formation of 1-NO-SG (Fig. S17). Upon excitation at 508 nm, a decrease of the fluorescence peak at 525 nm was accompanied by the increase of an emission band at 558 nm (Fig. 1b). In addition, the fluorescence intensity of 1 at 685 nm was significantly enhanced upon excitation at 660 nm (Fig. 1c). The above results validated that probe 1 can detect NO and GSH through three different fluorescence signals. We then examined the fluorescence intensity of 1 in the presence of different concentrations of NO and GSH. Upon excitation at 540 nm, there existed an excellent linear correlation between fluorescence intensity at 558 nm and GSH concentration from 0 to 50 μ M. The detection limit for GSH was estimated to be as low as 2.3×10^{-7} M (S/N = 3, Fig. 1d). Upon excitation at 660 nm, the emission intensity at 685 nm was linearly proportional to NO concentration in the 0–10 μ M range. The detection limit was determined to be 7.5×10^{-7} M (S/N = 3, Fig. 1e).

To examine selectivity, probe 1 was treated with other species. Upon excitation at 540 nm, an obvious fluorescence enhancement at 558 nm was observed in the presence of GSH, whereas the changes of fluorescence were negligible upon addition of other sulfur-containing salts and various amino acids (Fig. 1f). On the other hand, upon excitation at 660

nm, only NO induced a remarkable fluorescence increase at 685 nm (Fig. 1f). By comparison, there was no fluorescence signal with the addition of other RNS and ROS. These results indicate that probe 1 is suitable for NO and GSH detection without the interference of other biologically reactive species. In addition, we further confirmed that pH ranging from 6 to 8 would not affect the performance of the probe for imaging NO and GSH in biological environments (Fig. S2).

2.3. Distinct fluorescence signals revealed by *In Vitro* imaging of living cardiomyocytes

Inspired by the excellent spectral response of 1 towards NO and GSH in solutions, its ability of fluorescent imaging toward cellular NO and GSH was next investigated. Here, the H9C2 line of embryonic rat cardiomyocytes was employed as the model. The cytotoxicity of 1 in cells was first measured by Cell Counting Kit-8 (CCK8) assay, suggesting low cytotoxicity and good biocompatibility of 1 towards H9C2 cells (Fig. S3). As shown in Fig. 2a, when H9C2 cells were incubated with NEM (a GSH scavenger) and then 1, strong fluorescence in the probe channel was observed, but negligible fluorescence in the GSH and NO channels was detected under identical conditions. When H9C2 cells were only pretreated with 1, marked fluorescence was detected in the GSH channel while the fluorescence in the NO channel was negligible (Fig. S4). Meanwhile, an obvious decrease of the ratiometric signal between probe and GSH channels was also achieved (Fig. S5). As illustrated in Fig. S6, when NEM-pretreated H9C2 cells were incubated with DEA-NONOate and further loaded with 1, the NO channel exhibited a significant fluorescence enhancement and there was no fluorescence signal in the GSH channel. As time went by, the fluorescence intensity in the GSH channel increased gradually, demonstrating that the addition of exogenous NO stimulated GSH enhancement in H9C2 cells. After incubation with DEA-NONOate and then 1, GSH channel fluorescence increased while the signal for the probe channel diminished (Fig. S7), and a lower $F_{\text{probe}}/F_{\text{GSH}}$ ratio value was observed (Fig. S8). These results indicate the real-time reaction between 1 and GSH in H9C2 cells. In addition, the NO channel exhibited a remarkable fluorescence enhancement, demonstrating that 1 reacted with exogenous NO in H9C2 cells (Fig. S7). In sum, these results demonstrated that exogenous NO and GSH imaging was achieved by probe 1 through monitoring the fluorescence changes of three channels.

To further examine the fluctuations of NO and GSH in the HFpEF process, H9C2 cardiomyocytes were treated with PA (palmitic acid) and L-NAME (N^{ω} -nitro- L-arginine methyl ester) to mimics the pathological environment. As shown in the first column of Fig. 2b, in normal H9C2 cells, addition of 1 led to an obvious native green fluorescence while negligible fluorescence was observed in the GSH and NO channels. In the PA/L-NAME group, we observed remarkable fluorescence signals in both GSH and NO channels after incubating cells with 1, demonstrating higher levels of NO and GSH in H9C2 cells incubated with PA/L-NAME than normal H9C2 cells (the second column of Fig. 2b). Most importantly, when we prolonged the incubation time to 2 h, a decrease of fluorescence ratio between green and red channels was observed in H9C2 cells, implying that 1 is capable of revealing the endogenous GSH dynamically (Fig. 2c–e). When H9C2 cells in the PA/L-NAME group were incubated with carboxyl-PTIO (NO scavenger) and then loaded with 1 (the third column of Fig. 2b), the fluorescence signal in the NO channel decreased significantly. Moreover, when the cells in PA/L-NAME group were incubated with NEM and further treated with 1 (the fourth column of Fig. 2b), distinct fluorescence quenching in the GSH channel was observed. As incubation time was prolonged to 2 h, the fluorescence intensity in the GSH channel increased gradually, showing that the concentration of GSH increased (Fig. S9). Combined with the above-mentioned results demonstrating that exogenous NO induced GSH enhancement, it was concluded that endogenously produced NO may have an influence on the induction of GSH in the PA/L-NAME group. These results fully demonstrated the obvious upregulation of

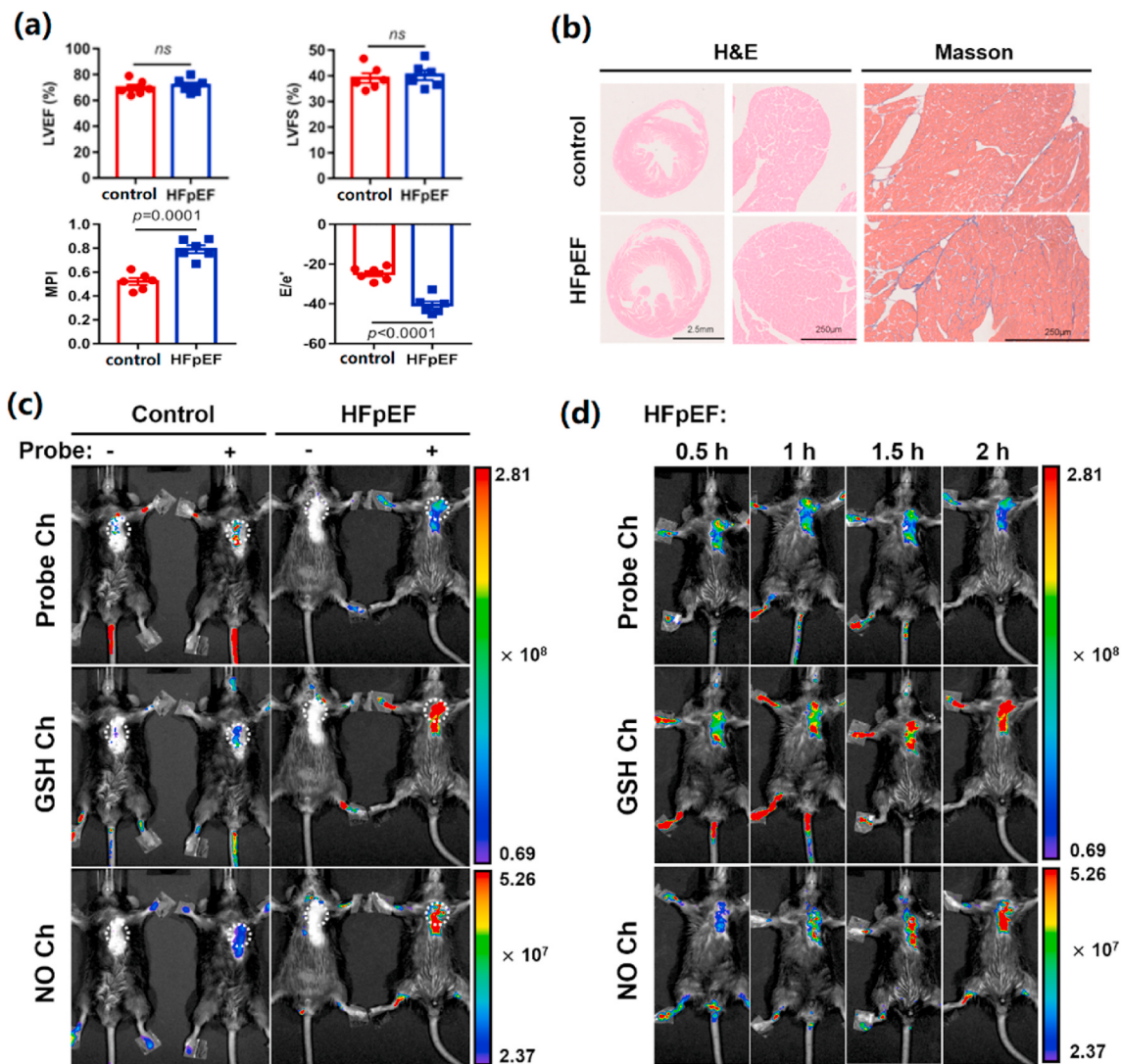


Fig. 3. Validation of a HFpEF Mouse Model and *in vivo* Fluorescence Imaging of Cardiac NO and GSH in HFpEF Mice. (a) Cardiac diastolic dysfunction in HFpEF mice revealed by echocardiography. LVEF, left ventricle ejection fraction; LVFS, left ventricular fractional shortening; MPI, myocardial performance index; E/e', ratio between mitral E wave and e' wave (E, peak Doppler blood inflow velocity across mitral valve during early diastole; e', peak tissue Doppler of myocardial relaxation velocity at mitral valve annulus during early diastole). (n = 5 mice per group, ns, not significant). (b) Representative images of hematoxylin & eosin (H&E) and Masson's Trichrome (MT) staining in transversal sections of heart after 15 weeks of diet. (c) Fluorescence images of normal or HFpEF model mice which were preinjected without or with probe 1 (40 μ M) for 2 h. (d) Fluorescence images of HFpEF model mouse after tail intravenous injection of probe 1 (40 μ M) at different time points. All of fluorescence images were acquired by an IVIS spectrum imaging system through three different sets of channels ($\lambda_{\text{ex}} = 500$ nm, $\lambda_{\text{em}} = 520$ nm; $\lambda_{\text{ex}} = 535$ nm, $\lambda_{\text{em}} = 560$ nm; $\lambda_{\text{ex}} = 640$ nm, $\lambda_{\text{em}} = 680$ nm).

GSH and NO in pathological cardiomyocytes, as well as the adequate sensitivity of probe 1 for targeted monitoring the change of NO and GSH with three different sets of fluorescence signals.

2.4. Verification of upregulation of cardiac NO and GSH in HFpEF mice by *In vivo* and *ex vivo* fluorescence imaging

The *in vivo* experiment of probe 1 for detecting NO and GSH was carried out in a HFpEF mouse model. A “two-hit” method, L-NAME in drink water and 60% High Fat Diet (HFD), was employed to construct the HFpEF mouse that can well mimic the clinical characteristics of HFpEF patients (Schiattarella et al., 2019). L-NAME can cause hypertension in mice, and 60% HFD can lead to metabolic disorder and obesity. As it turned out, both systolic and diastolic blood pressure elevated significantly at the 5th week of the above special diet (Figs. S10a and S10b), and the body weight of HFpEF mice emerged significant increase at 15th week (Fig. S10c). Most importantly, the

echocardiography results showed a cardiac diastolic dysfunction with normal ejection fraction in HFpEF mice (Fig. 3a and Fig. S10d). Furthermore, cardiac pathological analysis revealed an obvious cardiac hypertrophy and fibrosis (Fig. 3b and Figs. S10e–S10h). These results well confirmed the successful construction of HFpEF mice model. Subsequently, the *in vivo* imaging of GSH and NO using probe 1 was employed to assess the cardiac oxidative and nitrative stress in both control and HFpEF mice. Normal or HFpEF model mice were intravenously injected with buffer solutions containing 1 (40 μ M) and checked by fluorescence imaging after 2 h with an *in vivo* imaging system. As illustrated in Fig. 3c, without the injection of probe 1, both the control and HFpEF mice did not show any fluorescence signal. Stronger fluorescence intensity in probe channel was observed in normal mice with 1 than in HFpEF mice, suggesting that more probe 1 was consumed in HFpEF mice. For GSH imaging, the fluorescence intensity in GSH channel increased over time in HFpEF model mice with 1 (Fig. 3d). For NO imaging, the fluorescence in HFpEF mice increased gradually in NO

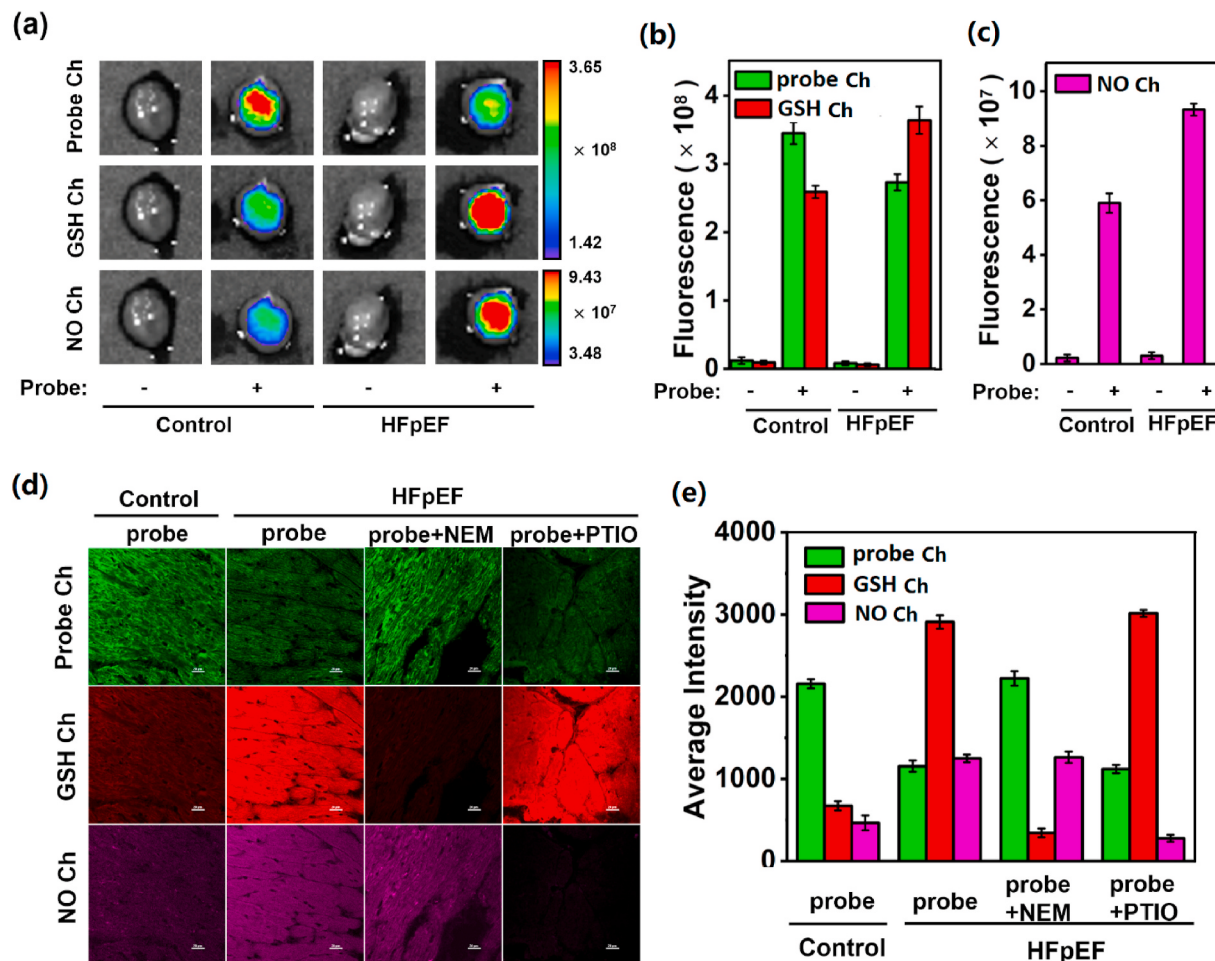


Fig. 4. Ex vivo Fluorescence Imaging of Cardiac NO and GSH in the isolated hearts and cardiac tissue slices. (a) Fluorescence images of harvested heart from a corresponding mouse sacrificed 2.5 h after probe 1 injection. (b, c) Fluorescence intensity at heart from normal (control) or HFP EF model mouse after tail intravenous without or with probe 1 (40 μ M) for 2.5 h. (d) Fluorescence images of cardiac slices from different mice: first column: normal issues incubated with probe 1 (40 μ M); second column: HFP EF-diseased slices treated with probe 1 (40 μ M); third column: HFP EF-diseased slices loaded with NEM (0.5 mM), and further stained with probe 1 (40 μ M); fourth column: HFP EF-diseased slices loaded with PTIO (0.5 mM), and further stained with probe 1 (40 μ M). (e) Average fluorescence intensity of probe, GSH and NO channels. Fluorescence images from green channel ($\lambda_{\text{ex}} = 487$ nm, $\lambda_{\text{em}} = 500\text{--}530$ nm), red channel ($\lambda_{\text{ex}} = 487$ nm, $\lambda_{\text{em}} = 557\text{--}590$ nm) and NIR channel ($\lambda_{\text{ex}} = 638$ nm, $\lambda_{\text{em}} = 670\text{--}720$ nm). Scale bar: 20 μ m.

channel, while weaker fluorescence was recorded in normal mice (Fig. 3c 3d). The above results demonstrated that the mice with HFP EF possessed more abundant NO and GSH than normal mice, which also suggested that obvious cardiac oxidative and nitritative stress had been implicated in the pathogenesis of HFP EF.

Next, the heart organs of experimental mice were isolated to perform the *ex vivo* fluorescence imaging. It can be seen that the fluorescence signal from heart organs of HFP EF mice was indeed higher than that from healthy mice in GSH and NO channel (Fig. 4a-c), which is consistent with the results acquired *in vivo*. Furthermore, the fluorescence images of cardiac sections loaded with probe 1 were analyzed. As shown in Fig. 4d and e, normal slices pretreated with 1 displayed a dramatic fluorescence intensity in green channel together with weak fluorescence signals in the red and NIR channels. For HFP EF-diseased slices incubated with 1, a remarkable fluorescence decreases in the probe channel was observed, and the images from GSH and NO channels showed significant fluorescence increases, demonstrating higher NO and GSH concentration in the HFP EF-diseased group than the normal group. To further investigate the corresponding fluorescence responses caused by the elevated levels of NO and GSH, two more experiments were performed. First, when HFP EF-diseased slices were treated with NEM and subsequently incubated with 1, it was found that scavenging GSH significantly decreased the fluorescence intensity in the GSH channel, while

the fluorescence intensity in the probe channel increased. Therefore, the fluorescence enhancement in the GSH channel was ascribed to the reaction between 1 and GSH in mice heart slices with HFP EF. Second, HFP EF-diseased slices incubated with PTIO (NO scavenger) and 1 showed weak emission intensity in the NIR channel, demonstrating that the high NO level in mice heart slices with HFP EF triggered the fluorescence response of 1. Taken together, we utilized a three-channel probe 1 to simultaneously visualize the higher concentration of NO and GSH in HFP EF mice *in vivo* for the first time, which might serve as an effective tool for exploring the pathology and therapeutic mechanisms of HFP EF.

2.5. Visualization of signaling pathways related to nitric oxide and glutathione in HFP EF

To reveal the important roles of NO and GSH in the pathological process of HFP EF, we further explored the underlying mechanism on the upregulation of GSH and NO in HFP EF mice. It has been reported that nitric oxide synthase (NOS) can use L-arginine as the substrate to generate NO and L-citrulline *in vivo* (Lundberg et al., 2015). This synthase exists three isoforms, including endothelial NOS (eNOS), neural NOS (nNOS), and inducible NOS (iNOS). nNOS and eNOS are constitutively expressed, while iNOS is only expressed under cell stress and can

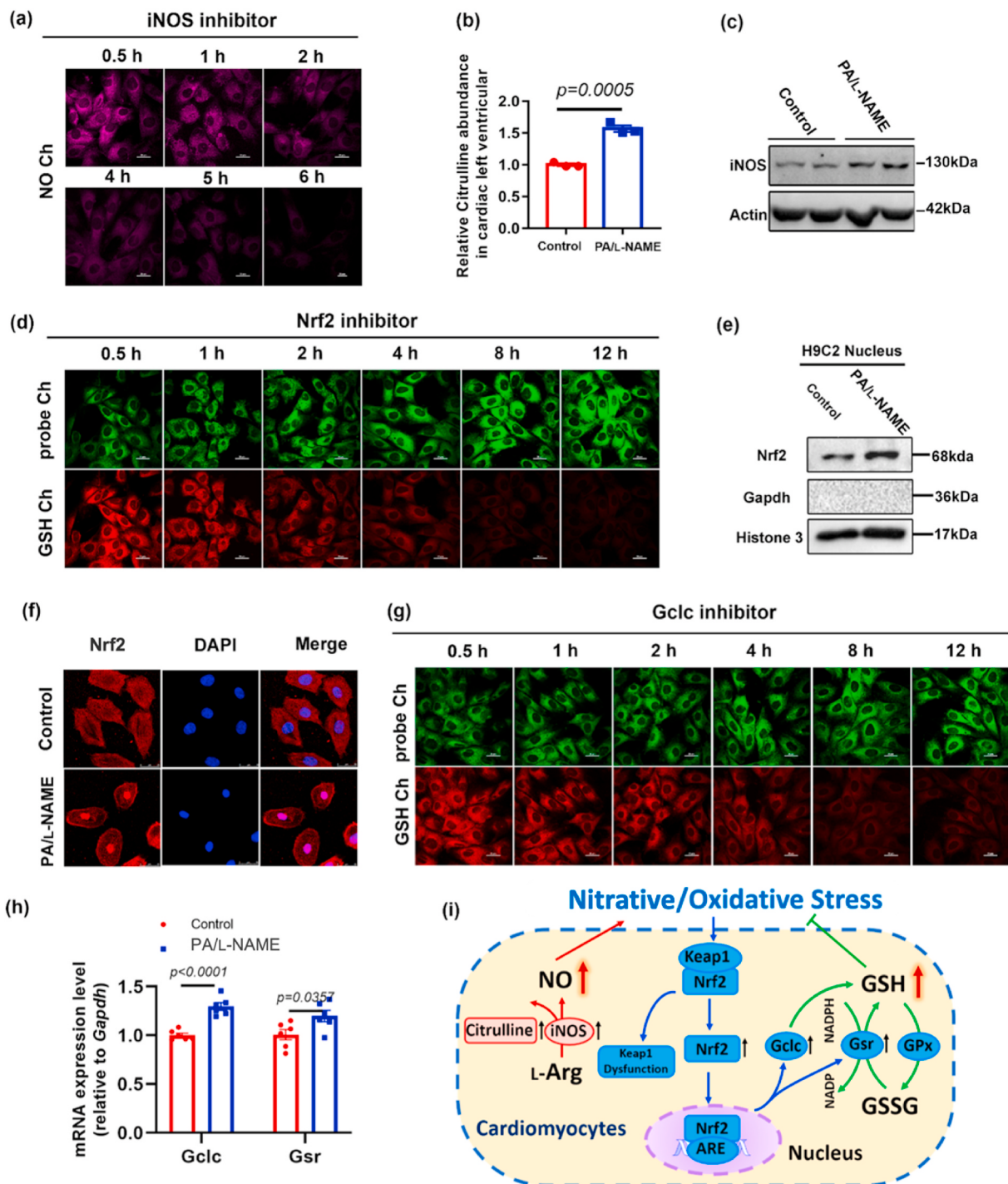


Fig. 5. Visualization of NO- and GSH-related signaling pathway in HFP EF. (a) Time-dependent confocal fluorescence imaging of H9C2 cells incubated with SMT (500 μ M), further treated with PA (100 μ M, 24 h) and L-NAME (100 μ M, 24 h), then loaded with 1 (10 μ M, 20 min). (b) Relative citrulline abundance in cardiac left ventricle from control and HFP EF mice. (c) Western blotting of iNOS in control and PA/L-NAME groups. (d) Time-dependent confocal fluorescence imaging of H9C2 cells incubated with ML385 (Nrf2 inhibitor, 20 μ M), further treated with PA (100 μ M, 24 h) and L-NAME (100 μ M, 24 h), then loaded with 1 (10 μ M, 20 min). (e) Nrf2 protein expression level in nucleus shown by subcellular fractionation and western blotting after 48 h treatment with PA and L-NAME in H9C2 cells. (f) Anti-Nrf2 immunofluorescence after 48 h treatment with PA and L-NAME in H9C2 cells. (g) Real-time confocal fluorescence imaging of H9C2 cells incubated with BSO (Gclc inhibitor, 500 μ M), further treated with PA (100 μ M) and L-NAME (100 μ M) for 24 h, then loaded with probe 1 (10 μ M, 20 min). (h) mRNA expression levels of Gclc and Gsr in NC and PA/L-NAME groups. (i) Schematic illustration of the signaling pathway underlying the up-regulation of NO and GSH in the HFP EF heart. Fluorescence images from probe channel ($\lambda_{\text{ex}} = 487$ nm, $\lambda_{\text{em}} = 500\text{--}530$ nm), GSH channel ($\lambda_{\text{ex}} = 487$ nm, $\lambda_{\text{em}} = 557\text{--}590$ nm) and NO channel ($\lambda_{\text{ex}} = 638$ nm, $\lambda_{\text{em}} = 670\text{--}720$ nm). Scale bar: 20 μ m.

generate large amounts of NO. To date, clinical trials have been largely unsuccessful in identifying effective treatments for HFpEF. The increase of endothelial NO caused by eNOS dysfunction is regarded as a pathogenic factor for HFpEF, while some clinical trials show that elevating cardiac NO production does not alleviate the symptom of HFpEF patients (Redfield et al., 2015). Thus, it was speculated that the clinical trials fail likely in connection with the activation of iNOS in cardiomyocytes. In the recent study, it has been proved firmly that the increased activity of iNOS from cardiomyocytes induces dramatically cardiac nitrative stress, thereby driving HFpEF (Schiaffarella et al., 2019). Thus, it was supposed that the enhanced fluorescence in NO channel may be due to the activation of iNOS in cardiomyocytes of HFpEF. As illustrated in Fig. 5a and Fig. S11a, when H9C2 cells in the PA/L-NAME group were incubated with SMT (S-methylisothiourea sulfate, a highly selective inhibitor for iNOS) (Heemskerk et al., 2009; Li et al., 2012) and 1, the fluorescence intensity in the NO channel decreased gradually. Metabolomics data based on LC-MS/MS showed that citrulline abundance was obviously upregulated in HFpEF heart (Fig. 5b). Furthermore, it had been observed that the expression level of iNOS was elevated in H9C2 cell line after stimulation by PA and L-NAME (Fig. 5c). These results demonstrate that the expression of iNOS induced a substantial increase of NO levels in HFpEF (Fig. 5i). Since iNOS is a critical factor of the pathophysiology of HFpEF, therapeutic strategies targeting a reduction in the activation of iNOS might hold promise for the treatment of HFpEF. Our probe may offer a useful chemical tool to evaluate therapeutic effect of future treatments by *in situ* monitoring NO level.

On the other hand, the mechanism underlying GSH upregulation was investigated. The elevation of GSH level is compensatory mechanism for the protection of cardiomyocytes against oxidative stress, the similar results has been reported in astrocytes (Oliveira et al., 2018). Many studies have well documented that nuclear factor erythroid 2-related factor 2 (Nrf2), as an important antioxidant transcription factor, participates in the regulation of GSH production (Brewer et al., 2011; Hybertson and Gao, 2014; Ian, 2006; James et al., 2008; Kalinina and Gavriluk, 2020; Kobayashi et al., 2016). To recapitulate briefly, Nrf2 binds to Kelch-like ECH-associated protein 1 (Keap1) in the cytosol in normal physiological condition, while the exposure of oxidative stress promotes Nrf2 escaping from the control of Keap1 to the nucleus. Subsequently, through the binding with the antioxidant response element (ARE), Nrf2 can upregulate both γ -glutamylcysteine synthase (Gclc) and glutathione reductase (Gsr), thereby elevating GSH production. However, it remains to be elucidated whether the Keap1/Nrf2/ARE pathway regulates cardiac GSH production in HFpEF. To confirm whether Nrf2 participates in the process of generating GSH, we treated the cells with ML385 (a selective Nrf2 inhibitor) (Hitzel et al., 2018; Qiu et al., 2020). H9C2 cells in the PA/L-NAME group pretreated with ML385 and 1 showed weaker emission intensity in the GSH channel while exhibiting stronger fluorescence intensity in the probe channel (Figs. 5d and S11c). In addition, western blotting and immunofluorescence were performed to evaluate the role of Nrf2 in HFpEF. We observed higher Nrf2 levels in the nucleus when the H9C2 cells are treated with PA/L-NAME (Fig. 5e). Compared with the normal group, immunofluorescence analysis demonstrated that Nrf2 in the PA/L-NAME group was transferred from the cytosol to the nucleus (Fig. 5f). In addition, under PA/L-NAME treatment, we incubated H9C2 cells with L-buthionine-sulfoximine (BSO, a specific Gclc inhibitor) (Drew and Miners, 1984) and further loaded with 1. Then, we observed a remarkable reduction of fluorescent intensity in GSH channel (Figs. 5g and S11b). Furthermore, we observed that the Gclc and Gsr levels were augmented in HFpEF through real-time quantitative polymerase chain reaction (RT-qPCR) (Fig. 5h). These results validated that Gclc and Gsr possessed the capability to regulate GSH production in our HFpEF model. The above results demonstrate that the Keap1/Nrf2/ARE pathway can activate the expression of Gclc and Gsr, thereby inducing the increase of GSH (Fig. 5i). Therefore, these results fully validated that upregulation of cardiac GSH was caused by

the activation of Keap1/Nrf2/ARE pathway in cardiomyocytes.

3. Conclusion

In summary, we successfully developed a fluorescent probe showing selective response to both NO and GSH with three different emission signals. Probe 1 itself exhibits green fluorescence ($\lambda_{em} = 525$ nm). In response to GSH and NO, 1 is converted to 1-NO-SG, switching on both red ($\lambda_{em} = 558$ nm) and NIR ($\lambda_{em} = 685$ nm) emission, which facilitates *in situ* monitor of NO and GSH levels. By using probe 1, cardiac oxidative and nitrative stress in the heart of HFpEF mice were clearly visualized by GSH and NO imaging. Moreover, probe 1 visualizes signaling pathways related to NO and GSH. On one hand, NO is induced by iNOS, which is a critical factor of the pathophysiology of HFpEF. On the other hand, GSH is mainly stimulated by Keap1/Nrf2/ARE signaling pathway in HFpEF. Thus, the present study not only propose a new pathway for distinguishing normal and HFpEF mice from a perspective of evaluating cardiac oxidative and nitrative stress, but also may contribute to guide and improve the treatment for HFpEF by expounding the mechanism. The probe provides a promising molecular imaging tools to visualize other biological and pathological process related to oxidative and nitrative stress *in vivo*.

CRediT authorship contribution statement

Xiao-Xiao Chen: Validation, Formal analysis, Investigation, Writing – original draft, Software. **Yufei Wu:** Validation, Formal analysis, Software, Writing – review & editing. **Xiaoxiao Ge:** Writing – review & editing. **Liandi Lei:** Validation, Software. **Li-Ya Niu:** Conceptualization, Methodology, Supervision, Data curation, Writing – review & editing, Visualization, Funding acquisition. **Qing-Zheng Yang:** Conceptualization, Methodology, Supervision, Funding acquisition. **Lemin Zheng:** Conceptualization, Supervision, Funding acquisition.

Declaration of competing interest

The authors declare that they have no known competing financial interests or personal relationships that could have appeared to influence the work reported in this paper.

Acknowledgements

This work was financially supported by the National Natural Science Foundation of China (21525206 and 21971023) to Q.-Z.Y., and State Commission of Science Technology of China (2020YFA0803700), National Natural Science Foundation of China (91639108, 81770272 and 81970425), Hangzhou Qianjiang Distinguished Expert Project to L.M.Z.

Appendix A. Supplementary data

Supplementary data to this article can be found online at <https://doi.org/10.1016/j.bios.2022.114510>.

References

- Bhuniya, S., Maiti, S., Kim, E.-J., Lee, H., Sessler, J.L., Hong, K.S., Kim, J.S., 2014. *Angew. Chem., Int. Ed.* 53 (17), 4469–4474.
- Birben, E., Sahiner, U.M., Sackesen, C., Erzurum, S., Kalayci, O., 2012. *World Allergy Organ. J.* 5 (1), 9–19.
- Boens, N., Leen, V., Dehaen, W., 2012. *Chem. Soc. Rev.* 41 (3), 1130–1172.
- Borlaug, B.A., 2014. *Nat. Rev. Cardiol.* 11 (9), 507–515.
- Borlaug, B.A., 2020. *Nat. Rev. Cardiol.* 17 (9), 559–573.
- Brewer, A.C., Murray, T.V.A., Arno, M., Zhang, M., Anilkumar, N.P., Mann, G.E., Shah, A. M., 2011. *Free Radical Biol. Med.* 51 (1), 205–215.
- Campos, J.C., Gomes, K.M.S., Ferreira, J.C.B., 2013. *Food Chem. Toxicol.* 62, 107–119.
- Chen, X., Wang, F., Hyun, J.Y., Wei, T., Qiang, J., Ren, X., Shin, I., Yoon, J., 2016. *Chem. Soc. Rev.* 45 (10), 2976–3016.
- Chen, X.-X., Niu, L.-Y., Shao, N., Yang, Q.-Z., 2019. *Anal. Chem.* 91 (7), 4301–4306.
- Chen, X.-X., Niu, L.-Y., Yang, Q.-Z., 2021. *Anal. Chem.* 93 (8), 3922–3928.

- Drew, R., Miners, J.O., 1984. *Biochem. Pharmacol.* 33 (19), 2989–2994.
- Dunlay, S.M., Roger, V.L., Redfield, M.M., 2017. *Nat. Rev. Cardiol.* 14 (10), 591–602.
- Erbas-Cakmak, S., Kolemen, S., Sedgwick, A.C., Gunnlaugsson, T., James, T.D., Yoon, J., Akkaya, E.U., 2018. *Chem. Soc. Rev.* 47 (7), 2228–2248.
- Fernández, A., Vendrell, M., 2016. *Chem. Soc. Rev.* 45 (5), 1182–1196.
- Finney, N., 2006. *Nat. Chem. Biol.* 2 (7), 349–350.
- Heemskerk, S., Masereeuw, R., Russel, F.G.M., Pickkers, P., 2009. *Nat. Rev. Nephrol.* 5 (11), 629–640.
- Hitzel, J., Lee, E., Zhang, Y., Bibli, S.I., Li, X., Zukunft, S., Pflüger, B., Hu, J., Schürmann, C., Vasconez, A.E., Oo, J.A., Kratzer, A., Kumar, S., Rezende, F., Josipovic, I., Thomas, D., Giral, H., Schreiber, Y., Geisslinger, G., Fork, C., Yang, X., Sigala, F., Romanoski, C.E., Kroll, J., Jo, H., Landmesser, U., Lusis, A.J., Namgaladze, D., Fleming, I., Leisegang, M.S., Zhu, J., Brandes, R.P., 2018. *Nat. Commun.* 9 (1), 2292.
- Huo, Y., Miao, J., Fang, J., Shi, H., Wang, J., Guo, W., 2019. *Chem. Sci.* 10 (1), 145–152.
- Hybertson, B.M., Gao, B., 2014. *Clin. Genet.* 86 (5), 447–452.
- Ian, A.B., 2006. *Curr. Drug Metabol.* 7 (8), 853–872.
- James, W.R., Muragundla, A., Alison, B.-S., 2008. *Curr. Drug Targets* 9 (1), 85–93.
- Jiang, X., Chen, J., Bajic, A., Zhang, C., Song, X., Carroll, S.L., Cai, Z.-L., Tang, M., Xue, M., Cheng, N., Schaaf, C.P., Li, F., MacKenzie, K.R., Ferreon, A.C.M., Xia, F., Wang, M.C., Maletić-Savatić, M., Wang, J., 2017. *Nat. Commun.* 8 (1), 16087.
- Kalinina, E.V., Gavriliuk, L.A., 2020. *Biochemistry (Moscow)* 85 (8), 895–907.
- Kang, Y.-F., Niu, L.-Y., Yang, Q.-Z., 2019. *Chin. Chem. Lett.* 30 (10), 1791–1798.
- Kobayashi, E.H., Suzuki, T., Funayama, R., Nagashima, T., Hayashi, M., Sekine, H., Tanaka, N., Moriguchi, T., Motohashi, H., Nakayama, K., Yamamoto, M., 2016. *Nat. Commun.* 7 (1), 11624.
- Kong, F., Liang, Z., Luan, D., Liu, X., Xu, K., Tang, B., 2016. *Anal. Chem.* 88 (12), 6450–6456.
- Li, W., Ren, G., Huang, Y., Su, J., Han, Y., Li, J., Chen, X., Cao, K., Chen, Q., Shou, P., Zhang, L., Yuan, Z.R., Roberts, A.I., Shi, S., Le, A.D., Shi, Y., 2012. *Cell Death Differ.* 19 (9), 1505–1513.
- Lim, M.H., Lippard, S.J., 2007. *Acc. Chem. Res.* 40 (1), 41–51.
- Lim, M.H., Xu, D., Lippard, S.J., 2006. *Nat. Chem. Biol.* 2, 375.
- Liu, H., Song, W., Zhang, S., Chan, K.S., Guo, Z., Shen, Z., 2020. *Chem. Sci.* 11 (32), 8495–8501.
- Liu, J., Sun, Y.-Q., Zhang, H., Shi, H., Shi, Y., Guo, W., 2016. *ACS Appl. Mater. Interfaces* 8 (35), 22953–22962.
- Lucero, M.Y., East, A.K., Reinhardt, C.J., Sedgwick, A.C., Su, S., Lee, M.C., Chan, J., 2021. *J. Am. Chem. Soc.* 143 (18), 7196–7202.
- Lundberg, J.O., Gladwin, M.T., Weitzberg, E., 2015. *Nat. Rev. Drug Discov.* 14 (9), 623–641.
- McDonagh, T.A., Metra, M., Adamo, M., Gardner, R.S., Baumbach, A., Böhm, M., Burri, H., Butler, J., Celutkienė, J., Chioncel, O., Cleland, J.G.F., Coats, A.J.S., Crespo-Leiro, M.G., Farmakis, D., Gilard, M., Heymans, S., Hoes, A.W., Jaarsma, T., Jankowska, E.A., Lainscak, M., Lam, C.S.P., Lyon, A.R., McMurray, J.J.V., Mebazaa, A., Mindham, R., Muneretto, C., Francesco Piepoli, M., Price, S., Rosano, G.M.C., Ruschitzka, F., Katherine Skibellund, A., Group, E.S.C.S.D., 2021. *Eur. Heart J.* 42 (36), 3599–3726.
- McQuade, L.E., Ma, J., Lowe, G., Ghatpande, A., Gelperin, A., Lippard, S.J., 2010. *Proc. Natl. Acad. Sci. USA* 107 (19), 8525.
- Mishra, S., Kass, D.A., 2021. *Nat. Rev. Cardiol.* 18 (6), 400–423.
- Morozumi, A., Kamiya, M., Uno, S.-n., Umezawa, K., Kojima, R., Yoshihara, T., Tobita, S., Urano, Y., 2020. *J. Am. Chem. Soc.* 142 (21), 9625–9633.
- Niu, L.-Y., Chen, Y.-Z., Zheng, H.-R., Wu, L.-Z., Tung, C.-H., Yang, Q.-Z., 2015. *Chem. Soc. Rev.* 44 (17), 6143–6160.
- Niu, L.-Y., Guan, Y.-S., Chen, Y.-Z., Wu, L.-Z., Tung, C.-H., Yang, Q.-Z., 2012. *J. Am. Chem. Soc.* 134 (46), 18928–18931.
- Oliveira, A.d.A.B., Melo, N.d.F.M., Vieira, É.d.S., Nogueira, P.A.S., Coope, A., Velloso, L.A., Dezonne, R.S., Ueira-Vieira, C., Botelho, F.V., Gomes, J.d.A.S., Zanon, R.G., 2018. *Neurochem. Int.* 120, 140–148.
- Park, S.-H., Kwon, N., Lee, J.-H., Yoon, J., Shin, I., 2020. *Chem. Soc. Rev.* 49 (1), 143–179.
- Qi, J., Feng, L., Zhang, X., Zhang, H., Huang, L., Zhou, Y., Zhao, Z., Duan, X., Xu, F., Kwok, R.T.K., Lam, J.W.Y., Ding, D., Xue, X., Tang, B.Z., 2021. *Nat. Commun.* 12 (1), 960.
- Qiu, Y.-b., Wan, B.-b., Liu, G., Wu, Y.-x., Chen, D., Lu, M.-d., Chen, J.-l., Yu, R.-q., Chen, D.-z., Pang, Q.-f., 2020. *Respir. Res.* 21 (1), 232.
- Redfield, M.M., Anstrom, K.J., Levine, J.A., Koeppl, G.A., Borlaug, B.A., Chen, H.H., LeWinter, M.M., Joseph, S.M., Shah, S.J., Semigran, M.J., Felker, G.M., Cole, R.T., Reeves, G.R., Tedford, R.J., Tang, W.H.W., McNulty, S.E., Velazquez, E.J., Shah, M.R., Braunwald, E., 2015. *N. Engl. J. Med.* 373 (24), 2314–2324.
- Sasaki, E., Kojima, H., Nishimatsu, H., Urano, Y., Kikuchi, K., Hirata, Y., Nagano, T., 2005. *J. Am. Chem. Soc.* 127 (11), 3684–3685.
- Schiattarella, G.G., Altamirano, F., Tong, D., French, K.M., Villalobos, E., Kim, S.Y., Luo, X., Jiang, N., May, H.I., Wang, Z.V., Hill, T.M., Mammen, P.P.A., Huang, J., Lee, D.I., Hahn, V.S., Sharma, K., Kass, D.A., Lavandero, S., Gillette, T.G., Hill, J.A., 2019. *Nature* 568 (7752), 351–356.
- Shah Amil, M., Claggett, B., Loehr Laura, R., Chang Patricia, P., Matsushita, K., Kitzman, D., Konety, S., Kucharska-Newton, A., Suetta Carla, A., Mosley Thomas, H., Wright Jacqueline, D., Coresh, J., Heiss, G., Folsom Aaron, R., Solomon Scott, D., 2017. *Circulation* 135 (3), 224–240.
- Su, D., Teoh, C.L., Wang, L., Liu, X., Chang, Y.-T., 2017. *Chem. Soc. Rev.* 46 (16), 4833–4844.
- Teng, L., Song, G., Liu, Y., Han, X., Li, Z., Wang, Y., Huan, S., Zhang, X.-B., Tan, W., 2019. *J. Am. Chem. Soc.* 141 (34), 13572–13581.
- Tian, M., Liu, X.-Y., He, H., Ma, X.-Z., Liang, C., Liu, Y., Jiang, F.-L., 2020a. *Anal. Chem.* 92 (14), 10068–10075.
- Tian, X., Li, Z., Ding, N., Zhang, J., 2020b. *Chem. Commun.* 56 (25), 3629–3632.
- Umezawa, K., Yoshida, M., Kamiya, M., Yamasoba, T., Urano, Y., 2016. *Nat. Chem.* 9, 279.
- Wang, S., Ren, W.X., Hou, J.-T., Won, M., An, J., Chen, X., Shu, J., Kim, J.S., 2021. *Chem. Soc. Rev.* 50 (16), 8887–8902.
- Wu, L., Huang, J., Pu, K., James, T.D., 2021. *Nat. Rev. Chem.* 5 (6), 406–421.
- Ye, M., Hu, W., He, M., Li, C., Zhai, S., Liu, Z., Wang, Y., Zhang, H., Li, C., 2020. *Chem. Commun.* 56 (46), 6233–6236.
- Yin, C.-X., Xiong, K.-M., Huo, F.-J., Salamanca, J.C., Strongin, R.M., 2017. *Angew. Chem. Int. Ed.* 56 (43), 13188–13198.
- Yin, J., Kwon, Y., Kim, D., Lee, D., Kim, G., Hu, Y., Ryu, J.-H., Yoon, J., 2015. *Nat. Protoc.* 10 (11), 1742–1754.
- Yu, X., Ge, L., Niu, L., Lian, X., Ma, H., Pang, L., 2018. *Oxid. Med. Cell. Longev.* 2018, 8364848.
- Yue, Y., Huo, F., Cheng, F., Zhu, X., Mafireyi, T., Strongin, R.M., Yin, C., 2019. *Chem. Soc. Rev.* 48 (15), 4155–4177.
- Zhou, T., Wang, J., Xu, J., Zheng, C., Niu, Y., Wang, C., Xu, F., Yuan, L., Zhao, X., Liang, L., Xu, P., 2020. *Anal. Chem.* 92 (7), 5064–5072.